Corrosion Science 140 (2018) 321–332

Contents lists available at ScienceDirect

Corrosion Science

journal homepage: www.elsevier.com/locate/corsci

Impact of oxidation of copper and its alloys in laboratory-simulated conditions on their antimicrobial efficiency

Monika Walkowicz[a,*], Piotr Osuch[a], Beata Smyrak[a], Tadeusz Knych[a], Ewa Rudnik[a], Łukasz Cieniek[b], Anna Różańska[c], Agnieszka Chmielarczyk[c], Dorota Romaniszyn[c], Małgorzata Bulanda[c]

[a] AGH University of Science and Technology, Faculty of Non-Ferrous Metals, Department of Metal Working and Physical Metallurgy of Non-Ferrous Metals, al. A. Mickiewicza 30, 30-059 Krakow, Poland
[b] AGH University of Science and Technology, Faculty of Metals Engineering and Industrial Computer Science, Department of Surface Engineering & Materials Characterisation, al. A. Mickiewicza 30, 30-059 Krakow, Poland
[c] Jagiellonian University Medical College, Faculty of Medicine, Department of Microbiology, ul. Czysta 18, 31-121 Krakow, Poland

ARTICLE INFO

Keywords:
A. Copper
B. Potentiostatic
B. SEM
C. Oxidation
C. Oxide coatings

ABSTRACT

Copper and its alloys are known for their antimicrobial activity, which makes them appealing materials for various touch surfaces in public facilities. These materials are also known for being prone to tarnishing, especially in contact with human palm sweat. The paper describes investigations on tarnishing of copper and various copper alloys by oxidation at elevated temperatures. After evaluation of thickness and chemical composition of oxide layers, microbiological tests were carried out in order to determine the impact of oxidation on antimicrobial efficiency of copper alloys.

1. Introduction

Almost 500 types of copper and its alloys have been approved by EPA [1] on the basis of laboratory tests and clinical trials as materials for antimicrobial touch surfaces. The challenge in the application of copper-based materials as touch surfaces is that the most of them are getting covered with corrosive oxide layers when exposed to human palm sweat or disinfecting agents used in healthcare facilities. For this reason, copper alloys that have high corrosion resistance due to the presence of alloy additives (Al, Ni, Zn) are the preferred choice in this type of applications [2]. On the other hand, in several publications [3–5], efficiency of various copper alloys in the elimination of selected bacteria (Gram positive and Gram negative) during microbiological tests, based mainly on JIS Z 2801 standard [6], has been compared. Michels et al. [7] reported that antimicrobial efficiency of copper-based touch surfaces depends mainly on the copper wt. % content in copper alloys. The authors also shown that antimicrobial efficiency is strongly associated with the corrosion resistance of material, concluding that with the increase in the corrosion resistance of copper alloy, the antimicrobial efficiency decreases. This phenomenon can be explained by fewer copper ions present on surface of such alloys. Copper ions [8–11] are responsible for eliminating bacteria by causing disruption of external and/or internal membrane of the bacteria, accumulation of copper ions in bacteria's cell, and in consequence, decomposition of bacteria DNA.

In case of copper alloys containing less noble metals, the oxides of alloying elements can be found in the oxide layer. The composition of the oxide layer very often does not correspond to the share of elements in the alloy. Generally, the less noble metals oxidize easier, hence their content in the surface oxide layer is higher than it could be concluded from the alloy composition. On the other hand corrosion products of copper alloys containing nobler metals contain mainly copper oxides. Depending on the temperature and time of atmospheric oxidation, copper oxide (II) CuO and/or copper (I) oxide Cu_2O are formed on surface of pure copper [12–14]. The composition and thickness of the oxide layer on the copper or its alloys after contact with human sweat or with hospitals disinfectants depends mainly on the chemical composition of metallic material, composition and pH of the solution reacting with the surface, as well as on the temperature and corrosion rate. For example, Fredj et al. [15] reported that after prolonged and repeated contact with a human palm sweat, a film of Cu_2O with thickness of about 50–230 nm on the surface of copper and its alloys

* Corresponding author.
E-mail addresses: monika.walkowicz@agh.edu.pl (M. Walkowicz), piotr.osuch@agh.edu.pl (P. Osuch), smyrak@agh.edu.pl (B. Smyrak), tknych@agh.edu.pl (T. Knych), erudnik@agh.edu.pl (E. Rudnik), lukasz.cieniek@agh.edu.pl (Ł. Cieniek), a.rozanska@uj.edu.pl (A. Różańska), agnieszka.chmielarczyk@uj.edu.pl (A. Chmielarczyk), d.romaniszyn@uj.edu.pl (D. Romaniszyn), malgorzata.bulanda@uj.edu.pl (M. Bulanda).

https://doi.org/10.1016/j.corsci.2018.05.033
Received 1 August 2017; Received in revised form 18 May 2018; Accepted 26 May 2018
Available online 30 May 2018

Table 1
Compositions (wt. %) of the investigated commercial copper alloys.

Common name	UNS code*	Cu	As	Fe	Mn	Al	Ni	P	Pb	Sb	Si	Sn	Zn
Copper (Cu-ETP)	C11000	99.9	0.0	0.002	0.001	0.0	0.0	0.030	0.002	0.000	0.008	0.0	0.0
Yellow Brass (CuZn37)	C27400	63.2	0.001	0.001	0.001	0.001	0.06	0.001	0.004	0.001	0.008	0.0	36.7
Tin Bronze (CuSn6)	C51900	94.1	0.006	0.001	0.001	0.016	0.01	0.222	0.038	0.001	0.002	5.5	0.1
Nickel silver (CuNi18Zn20)	C75200	63.1	0.001	0.027	0.12	0.001	17.9	0.001	0.001	0.008	0.001	0.001	18.9

was formed. He also showed that the thickness of oxide layer depends on the content of Cu in the alloy, concluding the higher the content of copper in alloy, the thicker the oxide layer is. There are also papers, in which authors utilized various chemical compositions of synthetic sweat for oxidation of copper and its alloys. For example, Harvey et al. [16] used a solution corresponding exactly to the chemical composition of human sweat, and defined its chemical stability. Often composition of synthetic sweat is based on industry standards EN 1811 [17], or ISO 3160 [18], in which synthetic formulas differ in composition, concentration and pH. Milosey et al. [19], showed that for copper alloy 62Cu-18Ni-20Zn (wt%), after 30 days of immersion in artificial sweat, the oxides layer was around 1000 nm thick, and consisted mainly of Cu_2O and ZnO. Colin et al. [20] additionally claim that the layer formed on the surface of copper alloys, in addition to Cu_2O contains also compounds based on Cl, and on alloys with high nickel content also Ni $(OH)_2$ and NiO were found. He also showed that for alloys rich in Cu (> 60%), chloride ions are present in the form of impurities in Cu_2O (copper chloride $CuCl_2$ and CuCl), while for alloys rich in Ni (> 60%), the secondary compound $Cu_2(OH)_3Cl$ was also found. These observations were confirmed by Procaccini et al. [21]. Analysis of corrosive layers formed on surfaces of monetary copper alloys (coper-nickel, nickel brass) as a result of their contact with synthetic sweat, is also the subject of many papers, for example, Elhadiri et al. [22]. From a literature review it can be concluded that the corrosion products of copper in contact with the human palm sweat, are similar to those observed after oxidation at elevated temperatures.

Several authors describe the influence of a corrosion surface layer on antimicrobial effectiveness of copper alloys. For example, Yeh et al. [23] reported that such effects exist. On the other hand, Michels et al. [24] showed that such influence does not exist. It can be concluded that the effect of the surface corrosion on antimicrobial efficiency of copper alloys is still not clear. Hence the purpose of current investigation was to determine the antimicrobial efficiency of copper and selected copper alloys in contact with the bacteria: Staphylococcus Aureus, and *Escherichia* Coli, after atmospheric oxidation in various temperatures. The study includes also characterization of corrosion surface layer by coulometric method, and scanning microscopy.

2. Materials and methodology

2.1. Materials

Commercial, high-purity copper and three representative copper alloys were selected for the study. Table 1 shows a list of materials with chemical composition (in wt. %) and their UNS (Unified Numbering System) code. From metal sheets, tapes or flat bars of copper and copper alloys, samples with dimensions of 0.5 mm x 20 mm x 20 mm were cut out. In order to remove corrosion inhibitor from their surfaces, samples were subjected to mechanical polishing and then chemical polishing in a mixture of concentrated acids: orthophosphoric (V) H_3PO_4, nitric(V) HNO_3, and acetic CH_3COOH, by volume at 3:1:1, at 25 °C. The material was cleaned with acetone in an ultrasonic bath and rinsed in distilled water.

2.2. Heat treatment and cathodic reduction of oxide layers

Atmospheric oxidation in an annealing furnace at the temperatures in the range of 200–600 °C for a duration of 1–60 minutes for ETP copper, and 1–24 h for copper alloys was carried out. The objective was to create superficial layers of copper oxide (I) with a thickness of 50–230 nm. According to Fredj et al. [15] similar layers are formed in contact with human palm sweat during regular use of copper based hardware in real life conditions.

Qualitative and quantitative composition of oxide layers was determined by coulometric method. For the investigations samples were connected to the electrolysis circuit as a cathode (0.785 cm^2 working

surface). The anode was a platinum wire. The electrolyte was 0.1 M Na_2SO_4 (20 cm^3). Measurements were taken at a temperature of 25 °C A cathodic reduction of oxide layers was conducted using a constant current density within a range of 0.1–1 mA/cm^2 (Autolab potentiostat/galvanostat, PGSTAT30). During the electrolysis, the cathode potential relative to a chlorine-silver reference electrode was recorded in one-second intervals.

During the electrolysis, on the cathode there is a reduction of M metal cation, contained in oxide:

$$M^{z+} + ze \rightarrow M \quad (1)$$

For example, for copper:

$$Cu^{2+} + 2e \rightarrow Cu \quad (2)$$

$$Cu^{+} + e \rightarrow Cu \quad (3)$$

Each oxide corresponds to a specific reduction cathodic potential (–0.74 V for CuO and –0.80 V for Cu_2O against saturated calomel electrode SCE). Completion of the reduction of individual compounds was indicated by a discrete change of cathode potential during electrolysis. The mass of metal in the form of an oxide was calculated using Faraday's law, based on current and time of cathodic reduction:

$$(m_M)_{M_xO_y} It_{M=\frac{M_M}{zF}{}_xO_y} \quad (4)$$

For example, for copper:

$$(m_{Cu})_{CuO}=\frac{M_{Cu}}{2F}It_{CuO} \quad (5)$$

and

$$(m_{Cu})_{Cu_2O}=\frac{M_{Cu}}{F}It_{Cu_2O} \quad (6)$$

Amounts of oxides forming the individual layers were calculated from metal amounts in various oxides:

$$m_{M_xO_y}=\frac{M_{M_xO_y}\bullet(m_M)_{M_xO_y}}{xM_M} \quad (7)$$

For example, for copper:

$$m_{CuO}=\frac{M_{CuO}\bullet(m_{Cu})_{CuO}}{M_{Cu}} \quad (8)$$

and

$$m_{Cu_2O}=\frac{M_{Cu_2O}\bullet(m_{Cu})_{Cu_2O}}{2M_{Cu}} \quad (9)$$

The thickness of the oxide film is the sum of thicknesses of individual oxide layers yy_{MxOy}, calculated according to the following formula:

$$y_{M_xO_y}=\frac{m_{M_xO_y}}{S\bullet d_{M_xO_y}} \quad (10)$$

For example, for copper:

$$y_{CuO}=\frac{m_{CuO}}{S\bullet d_{CuO}} \quad (11)$$

and

$$y_{Cu_2O}=\frac{m_{Cu_2O}}{S\bullet d_{Cu_2O}} \quad (12)$$

For calculations following oxides densities were used: 6.4 g/cm^3 for CuO and 6.0 g/cm^3 for Cu_2O.

2.3. Multipoint quantitative analysis (EDX multipoint) of the chemical composition in surface layers

Chemical composition analysis on subsurface layers cross-sections for all oxidized samples: Cu-ETP (300 °C, 1 h), CuZn37 (300 °C, 24 h), CuSn6 (200 °C, 24 h) and CuNi18Zn20 (300 °C, 24 h) were carried out using high resolution scanning electron microscope (FEI Nova NanoSEM 450) with EDX (SDD Apollo X) detector (by EDAX "GENESIS Multipoint" method). Mechanically polished metallographic samples revealed the cross-sectional structure of the oxidized subsurface layers as reaction products. Analysis were carried out on non-etched sections. Series of separate measurement points (100–150) for a full quantitative analysis were established individually for each analysed sample through oxidized layers starting from the metal core (with time step 40–60 s per point). Initially all samples were subjected to a general overview to expose oxide layers on cross-sections, and choose the best places for a subsequent, thorough analysis. Additionally, for selected areas, a qualitative analysis of the chemical distribution was carried out (maps of specified elements). All oxidized samples were analysed for the presence of selected elements: O (K series characteristic radiation) and Cu, Zn, Sn, Ni (K and L series characteristic radiation) with the following parameters: accelerating voltage 10 kV; beam current (spot): 3.5–4; WD = 4.8–5.0 mm. SEM observations were carried out with the use of two types of detectors: ETD - secondary electrons detector (SE) working in classic or immersion mode (UHR - ultra-high resolution), and CBS - a four-ring concentric detector of backscattered electrons (BSE).

2.4. Tests of antimicrobial properties

Samples of copper and its alloys, non-oxidized and after oxidation at elevated temperatures were tested for antimicrobial efficiency in relation to gram-positive and gram-negative bacteria strains. Before microbiological testing, the samples were cleaned by immersion in acetone and sterilized by wiping with 96% alcohol. Among the thermally treated materials (oxidized), antimicrobial efficiency tests were carried out on: ETP copper – C110 (300 °C, 1 h), brass CuZn37 – C274 (300 °C, 24 h), bronze CuSn6 – C519 (200 °C, 24 h), nickel-silver CuNi18Zn20 – C752 (300 °C, 24 h). Selection of the temperature and exposition time at elevated temperatures was based on oxide layers thickness comparison between own investigations on atmospheric oxidation and experiment on oxidation during contact with human palm sweat in real life conditions, reported in the literature [15].

In this study the modified methodology of Japanese Standard [6]) for assessing antimicrobial efficacy of non-porous materials was used. Microbiological testing was conducted using a bacterial suspension of Staphylococcus Aureus (SA) and *Escherichia* Coli (EC) prepared in saline and tryptic soy broth according to the formula described below. The tested bacterial strains were stored in glycerol at −70 °C. A day before antimicrobial efficacy testing, a small amount of the bacteria suspension was taken form a frozen sample, inoculated onto solid Muller-Hinton agar and then incubated for 24 h at 37 °C. From the obtained culture, a suspension was prepared in saline at a density of 0.5 McFarland standard controlled using a densitometer. Subsequently, 100 µL of the suspension with a density of 0.5 McFarland standard was transferred into 900 µL of TSB. Each time, a control of the viability of the bacteria obtained in the culture on solid medium and the control of the precise initial concentration (its density expressed in CFU/mL) was performed.

The test samples were placed in a sterile Petri dishes made of PVC with a capacity of 100 mL that was 6 cm in diameter, and then, 100 µL of the test suspension was applied on samples' surface. Next, the inoculum on samples' surface was covered with sterile polypropylene foil

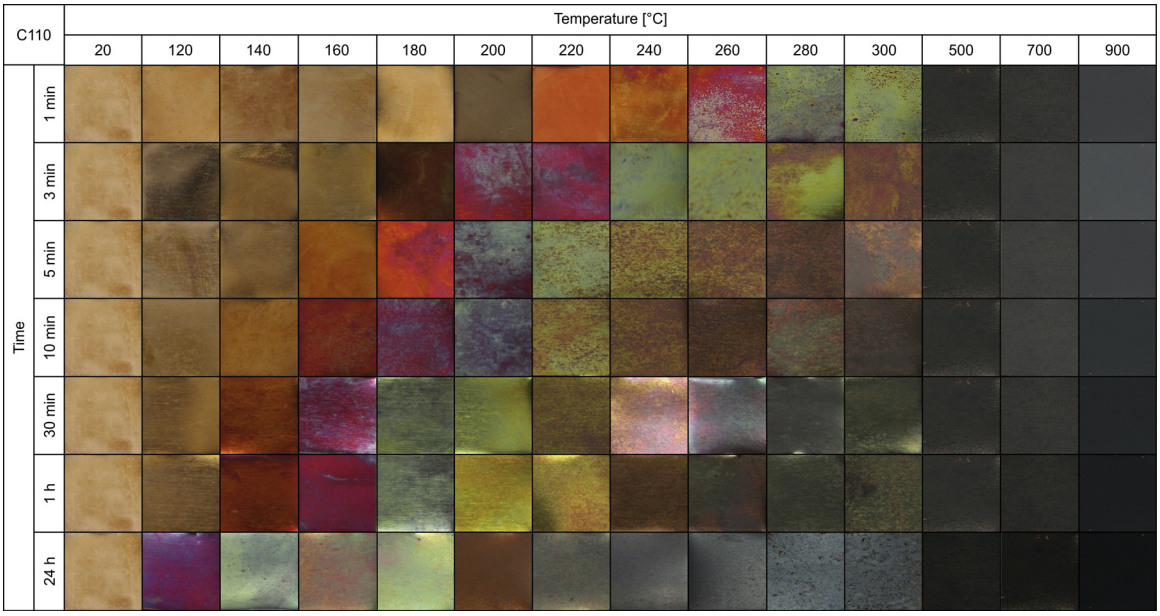

Fig. 1. Surfaces of Cu-ETP copper sheet samples (C11000) after atmospheric oxidation at elevated temperatures during various exposition time intervals.

measuring 2 cm × 2 cm to reduce surface tension. The Petri dishes were covered to prevent contamination of the sample with microbes from the air, but it remained loose enough that aerobic conditions were maintained throughout the course of exposure and when left for a specified period of time (0, 30, 60, 90, 120, 180, 240, and 300 min) at approx. 22 °C (room temperature).

After a certain period of time, 5 mL of the TSB solution and approx. 30 sterile glass beads that were 2 mm in diameter were placed into the container and shaken for 2 min in a shaker-incubator. Then, 100 µL of the wash was collected, 4 serial decimal dilutions were prepared, of which 100 µL was inoculated onto solid MHA for each time point. After a 24-hour incubation, individual colonies were counted on the plates when the resulting number was countable.

For each test materials, each exposure time for both microbes was repeated three times. To count the amount of CFU/mL after exposure of the bacterial suspension to the studied materials, the average of the triplicates was used. The formula for the calculation was:

$$\mathrm{CFU/ml} = \frac{(n \bullet f \bullet v_1)}{(v_2 \bullet v_3)} \tag{13}$$

where: n – average number of colonies/plate in dilution, f – dilution factor, v_1 – volume of TSB used for washing the bacteria that survived after exposure, v_2 – volume used and applied on metallic coupons, and v_3 – volume of the plated material ($v_{1\text{-}3}$ in mL).

To evaluate the antimicrobial efficiency, the criteria used by Souli et al. [25] were adopted according to which a suspension density reduction occurred, ranging from ≤ 2 to < 3 log mean bacteriostatic properties, as well as a reduction of over 3 log – bactericidal properties.

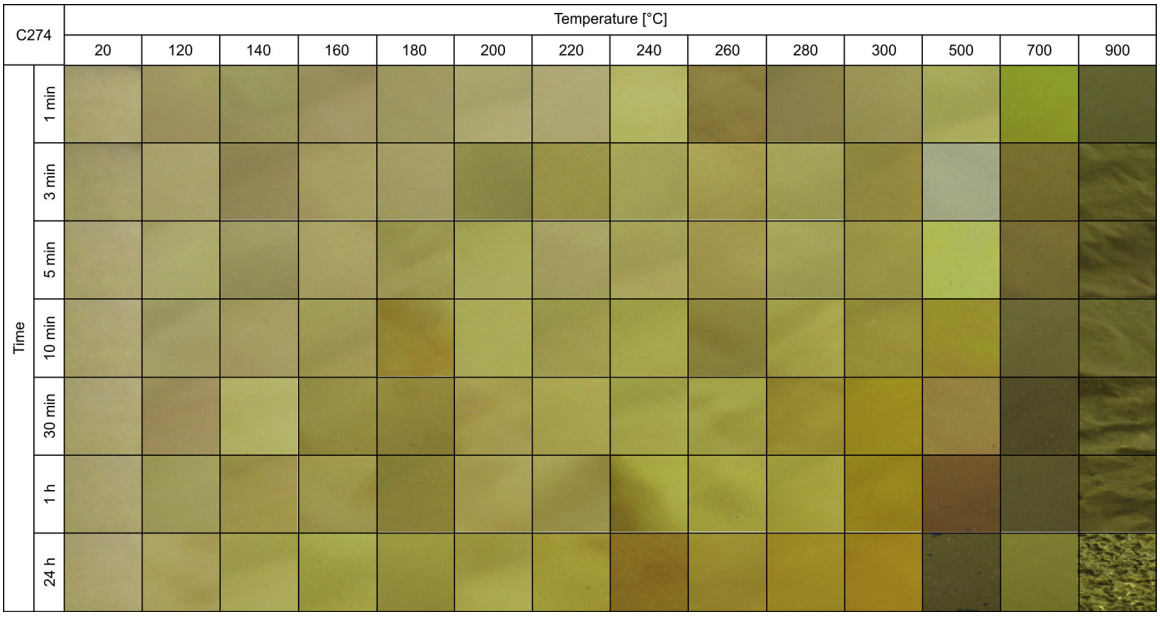

Fig. 2. Surfaces of brass sheet samples (C27400) after atmospheric oxidation at elevated temperatures during various exposition time intervals.

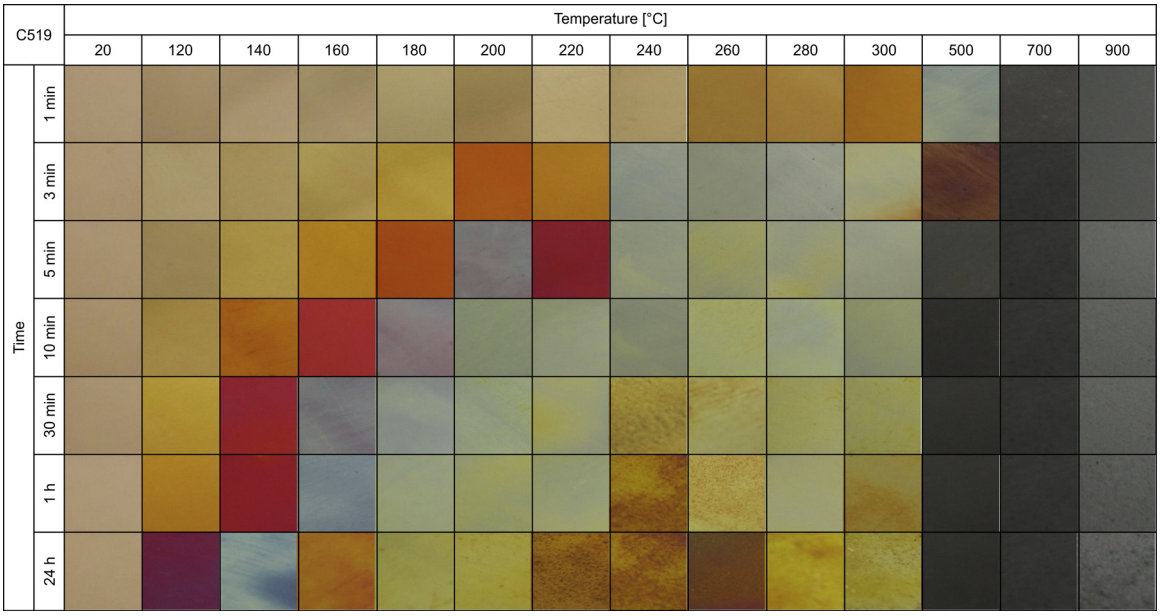

Fig. 3. Surfaces of tin bronze sheet samples (C51900) after atmospheric oxidation at elevated temperatures during various exposition time intervals.

3. Results and discussion

3.1. Visual assessment of oxidation products

Figs. 1–4 are showing surface of test materials subjected to atmospheric oxidation at elevated temperatures. Pictures of particular samples are set in pattern, which allows for visual assessment of corrosion products after heat treatment at specific temperature and given time interval. Oxidation of pure copper (Fig. 1) at elevated temperatures leads to formation of copper oxides with various appearance. It was found that the temperatures over 500 °C provide even, black surface, which is result of formation of copper (I) oxide Cu_2O. Similar surface can be obtained at much lower temperatures from 220 °C as well, but at much longer exposure time (24 h). At temperatures in a range from 120 up to 300 °C appearance of the samples vary, which is a result of various content of copper (I) oxide Cu_2O and copper (II) oxide CuO on the surface. It should be noted that time-temperature equivalent can be seen, as for example 120 °C/ 24 h and 180 °C/10 min. Very similar colours pattern can be observed for CuSn6 alloy, shown in Fig. 3, while alloys containing much higher amount of alloying elements changed their appearance very slightly, especially at lower temperatures. Detailed analysis of surface corrosion products formed on the test materials as a result of atmospheric oxidation is shown later in this paper.

3.2. Determination of oxides thickness by cathodic reduction

The curves illustrating potential E (V) vs. time (s) were examined for non-oxidized copper sample first, as is shown in Fig. 5. It was found that immediately after turning on the current, the cathode potential is reduced to below -0.9 V, then levelling off at ca. -1.2 V, characteristic for the emission of gas hydrogen on copper surface:

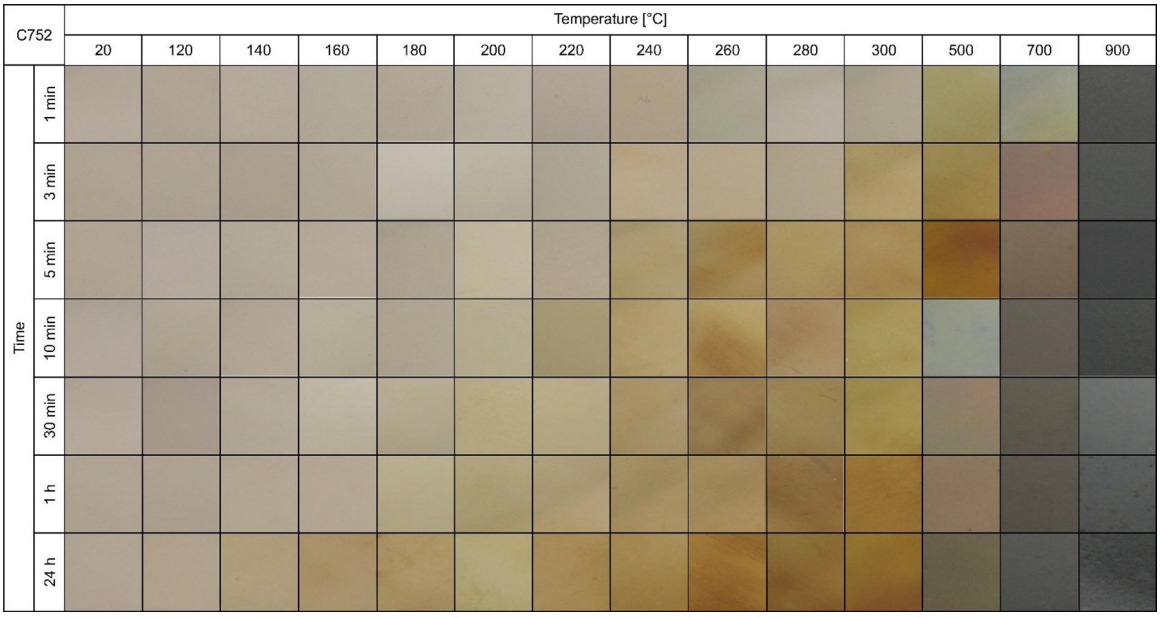

Fig. 4. Surfaces of nickel silver sheet samples (C75200) after atmospheric oxidation at elevated temperatures during various exposition time intervals.

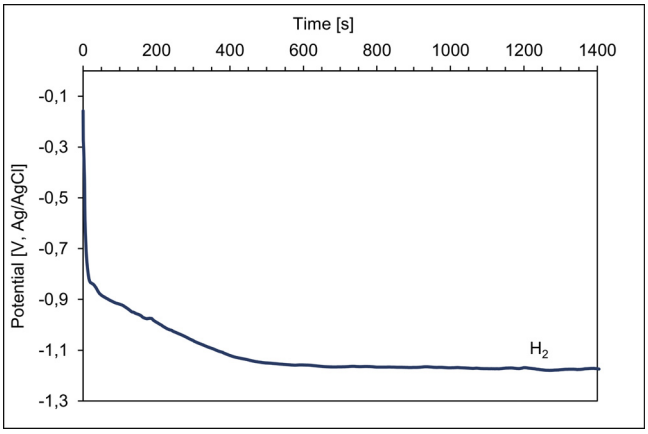

Fig. 5. Potential-time curve of cathodic reduction for a non-oxidised copper sample.

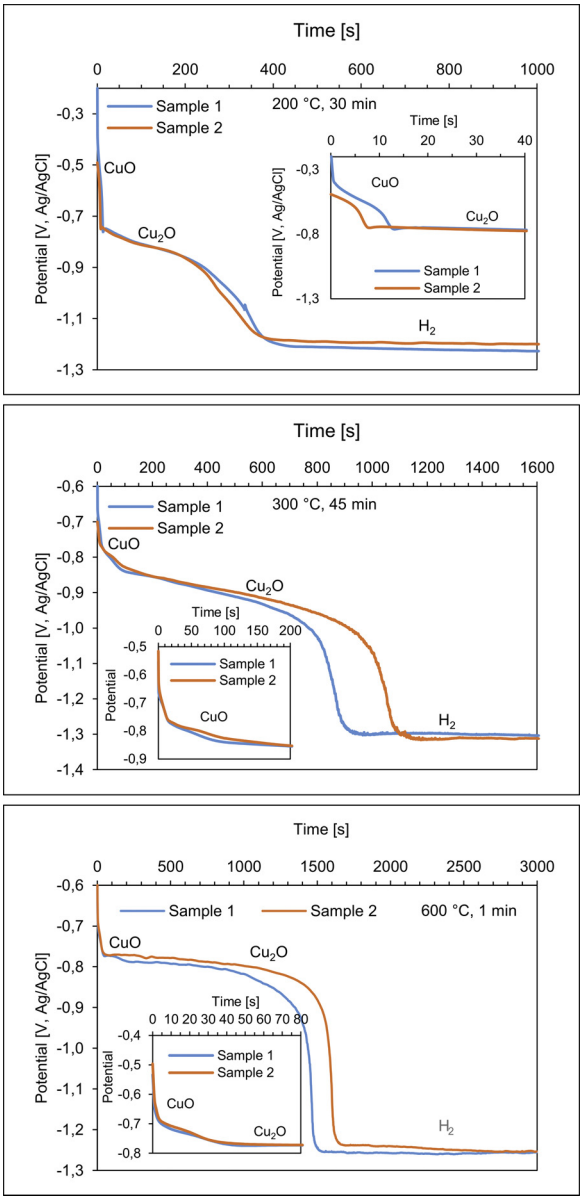

Fig. 6. Potential-time curves of cathodic reduction of copper oxides on copper surface at various temperatures and time of annealing.

Table 2
Results of coulometric analysis of oxide layers obtained for copper after annealing in various temperatures and times (results of coulometric research).

Oxidation		Current density, mA/cm^2	Time of cathodic reduction, s		Layer thickness, μm	
T, °C	t, min		Cu_2O	CuO	Cu_2O	CuO
200	1	0.5	80	–	0.04	–
		0.5	94	–	0.05	–
	5	0.5	177	–	0.11	–
		0.5	257	–	0.16	–
	30	0.5	376	13	0.23	0.004
		0.5	363	13	0.22	0.004
	60	1.0	215	3	0.27	0.002
250	5	0.5	648	18	0.40	0.006
		0.5	755	20	0.47	0.006
		0.5	927	28	0.57	0.009
	30	0.5	662	138	0.41	0.044
		0.5	784	176	0.48	0.057
	60	1.0	255	70	0.32	0.045
300	1	0.1	265	–	0.03	–
		0.25	360	–	0.11	–
	5	0.25	4665	285	1.44	0.046
		0.5	1085	215	0.67	0.069
		0.5	1525	425	0.94	0.137
	30	0.5	3892	108	2.40	0.035
	45	1.0	810	85	1.00	0.055
		1.0	995	100	1.23	0.064
400	1	0.5	250	–	0.16	–
		0.5	132	–	0.08	–
		0.5	192	–	0.12	–
600	1	1.0	1595	25	1.97	0.016
		1.0	1595	25	1.97	0.016
		1.0	1445	40	1.78	0.026
		1.0	2220	30	2.74	0.019

$$2H^+ + 2e \rightarrow H_2 \quad (14)$$

This fact indicates that on non-oxidised copper sample it is not possible to confirm the presence of oxide. Therefore, it was assumed to be non-existent.

Fig. 6 presents chronopotentiometric curves obtained for copper samples oxidised at various temperatures. It was found that depending on the temperature and time of thermal treatment, the curves show one or two potential drops resulting from the presence of, respectively: one (Cu_2O) or two oxides (Cu_2O and CuO). In each case, the measurement ended in reaching the plateau associated with the reaction (14). Detailed results of measurements are summarised in Table 2. It is observed that the total thickness of the oxide layer (CuO and Cu_2O) formed on the surface of copper during 1 min oxidation process increases from 44 nm for a sample annealed at a temperature of 200 °C to almost 2000 nm - for copper annealed at a temperature of 600 °C.

In case of copper alloys coulometric measurements were taken for metals being alloying elements, first: Ni, Zn and Sn non-treated thermally, and oxidised at temperatures of 200 °C or 300 °C. The results are shown in Fig. 7 (left column) and in Table 3.

For nickel, immediately after turning on the power for electrolysis, the cathode potential decreases, then is set at a constant level of ca. -1.2 V for non-oxidised metals, -1.4 V in metals oxidised in 300 °C for 1 h, and -1.5 V for metal oxidised in 300 °C for 24 h. In each case, the time period, which may correspond to the reduction of oxide ranges from 25 s for samples non thermally treated to 100 s for sample oxidized for 24 h. It was assumed that at these oxidation parameters only NiO is formed (NiO is the only oxide forming on nickel oxidized at temperatures below 700 °C). Process of reduction of nickel ions contained in NiO that occurs during electrolysis can be described by the following formula:

$$Ni^{2+} + 2e \rightarrow Ni \quad (15)$$

which was adopted as the basis for the calculation of the oxide layer

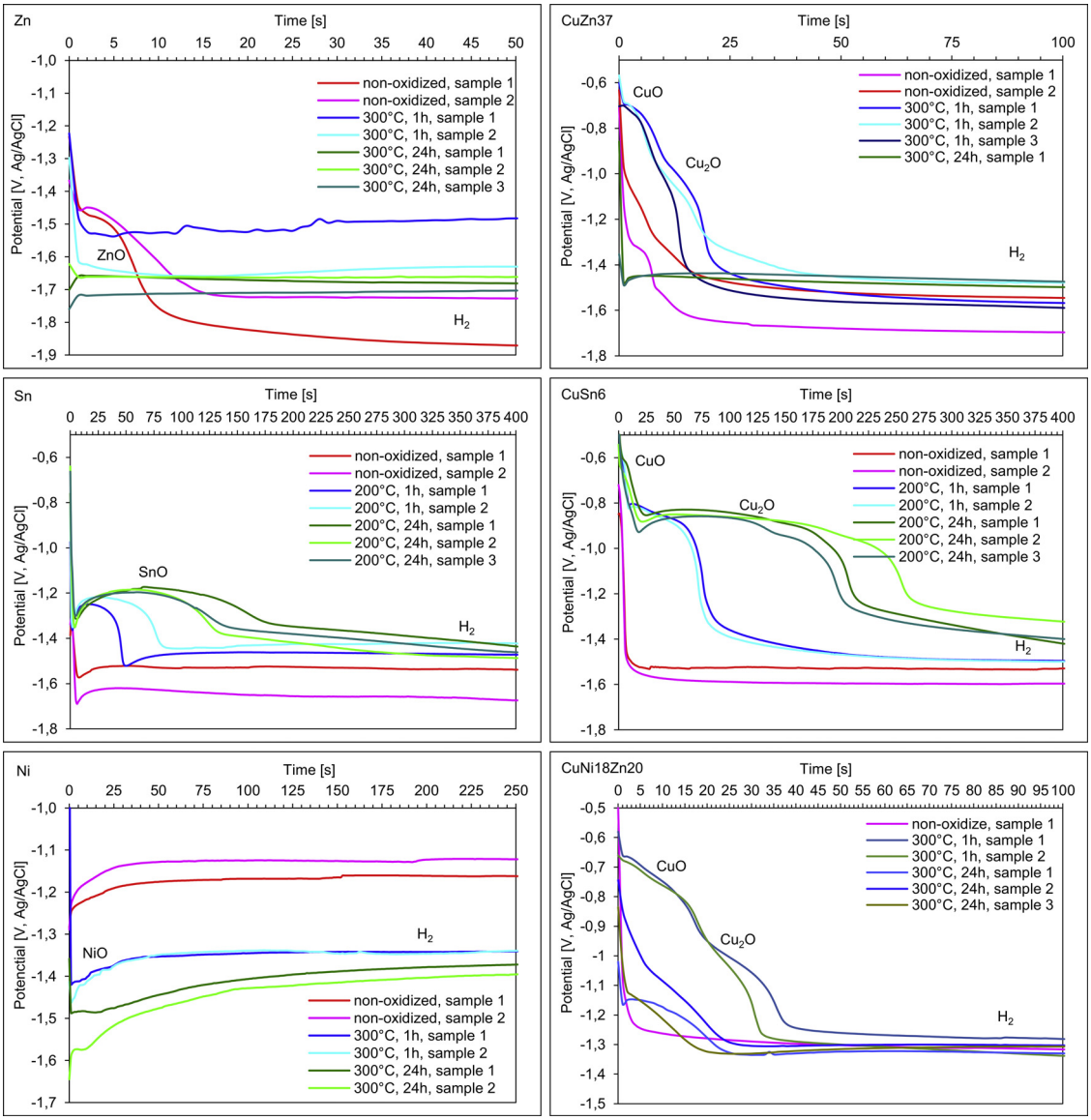

Fig. 7. Potential-time curves of cathodic reduction of copper oxides on copper alloys surfaces after oxidation at various temperature and time.

Table 3
Results of coulometric analysis of oxide layers obtained on pure metals at various temperature and time.

Metal	Oxidation		Oxide reduction time, s	Metal weight in oxide, g	Oxide weight, g	Oxide layer thickness, nm	Average oxide layer thickness, nm
	T, °C	t, h					
Ni	–	–	27	$6.45 \cdot 10^{-6}$	$8.20 \cdot 10^{-6}$	140	148 ± 11
			30	$7.16 \cdot 10^{-6}$	$9.12 \cdot 10^{-6}$	155	
	300	1	40	$9.55 \cdot 10^{-6}$	$1.22 \cdot 10^{-5}$	207	197 ± 15
			36	$8.60 \cdot 10^{-6}$	$1.09 \cdot 10^{-5}$	187	
	300	24	94	$2.24 \cdot 10^{-5}$	$2.86 \cdot 10^{-5}$	487	497 ± 15
			98	$2.34 \cdot 10^{-5}$	$2.98 \cdot 10^{-5}$	508	
Sn	–	–	5	$2.41 \cdot 10^{-6}$	$4.16 \cdot 10^{-6}$	82	78 ± 6
			4.5	$2.17 \cdot 10^{-6}$	$3.75 \cdot 10^{-6}$	74	
	200 °C	1	46	$2.22 \cdot 10^{-5}$	$3.83 \cdot 10^{-5}$	756	1044 ± 407
			81	$3.91 \cdot 10^{-5}$	$6.74 \cdot 10^{-5}$	1332	
	200 °C	24	153	$7.39 \cdot 10^{-5}$	$1.27 \cdot 10^{-4}$	2516	2639 ± 174
			168	$8.11 \cdot 10^{-5}$	$1.40 \cdot 10^{-4}$	2763	
Zn	–	–	15	$3.99 \cdot 10^{-6}$	$4.97 \cdot 10^{-6}$	113	94 ± 27
			10	$2.66 \cdot 10^{-6}$	$3.31 \cdot 10^{-6}$	75	
	300	1	145	$3.86 \cdot 10^{-5}$	$4.80 \cdot 10^{-5}$	1090	1090
	300 °C	24	560	$1.49 \cdot 10^{-4}$	$1.85 \cdot 10^{-4}$	4210	4398 ± 266
			610	$1.62 \cdot 10^{-4}$	$2.02 \cdot 10^{-4}$	4586	

Table 4
Results of coulometric analysis of oxide layers obtained on surface of copper alloys at various temperature and time.

Alloy	Oxidation		Oxide reduction time, s		Cu weight in the oxide, 10^{-6} g		Oxide weight, 10^{-6} g		Oxide layer thickness, nm	
	T, °C	t, h	CuO	Cu_2O	CuO	Cu_2O	CuO	Cu_2O	CuO	Cu_2O
CuZn37			–	9	–	4.65	–	5.23	–	11.1
			–	12	–	6.20	–	6.98	–	14.8
	300	1	10	11	2.58	5.66	3.23	6.40	6.4	13.6
			8	14	2.06	7.23	2.59	8.14	5.1	17.3
			8	7	2.06	3.61	2.59	4.07	5.1	8.6
	300	24	330	480	85	248	107	279	212	593
			390	400	101	207	126	233	251	494
CuNi18Zn20	–	–	–	1.5	–	0.77	–	0.87	–	1.9
	300	1	19	19	4.91	9.82	6.14.	11.05	12.2	23.5
			20	12	5.16	6.20	6.47	6.98	12.9	14.8
	300	24	–	24	–	12.4	–	13.96	–	29.6
			–	24	–	12.4	–	13.96	–	29.6
			–	16	–	8.27	–	9.31	–	19.8
CuSn6	–	–	–	7	–	3.66	–	4.13	–	8.8
			–	6	–	3.30	–	3.72	–	7.9
	200	1	8	74	2.06	3.82	2.59	43.0	5.1	91.4
			8	71	2.06	3.66	2.59	41.3	5.1	87.7
	200	24	19	201	4.91	104	6.14.	117	12.2	248
			15	250	3.87	129	4.85	145	9.7	309
			12	198	3.09	102	3.88	115	7.7	245

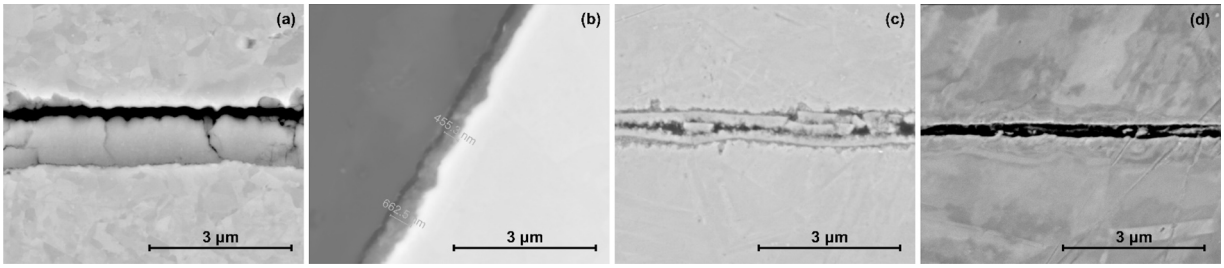

Fig. 8. SEM images after oxidation: (a) C11000, (b) C27400, (c) C51900, and (d) C75200.

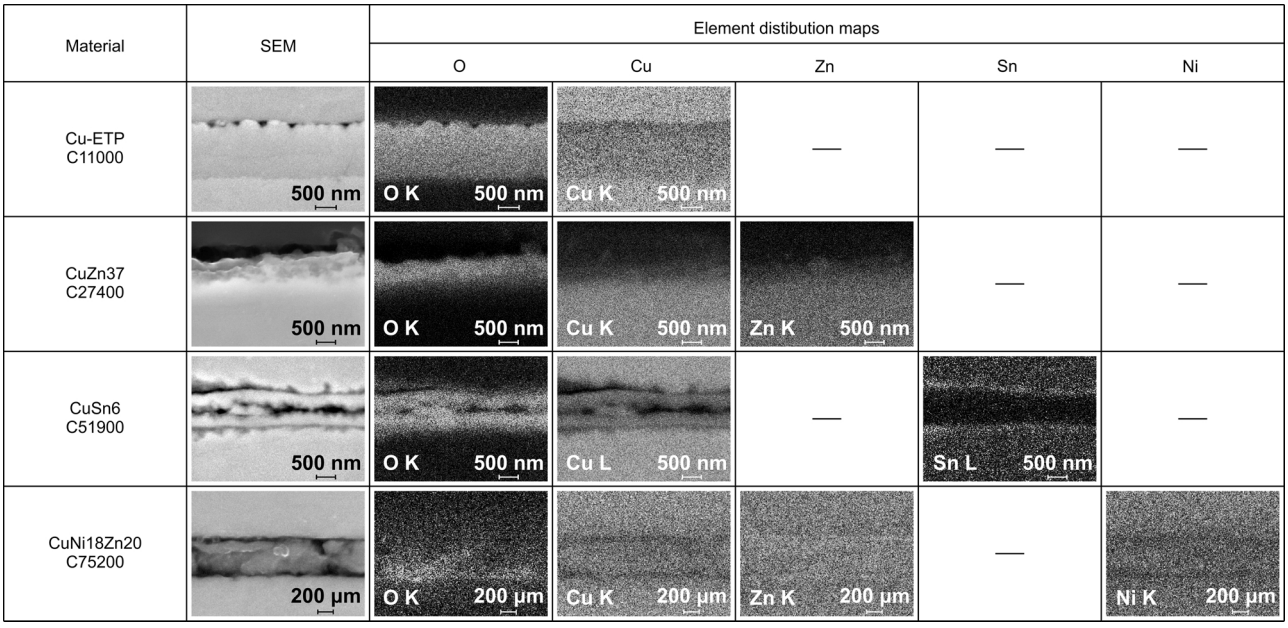

Fig. 9. Distribution maps of elements for C11000, C27400, C51900, and C75200 samples.

thickness by Eqs. (4) and (7), where $d_{NiO} = 7.45\,g/cm^3$. The results show that NiO thickness change from 147 ± 11 nm (natural oxide layer) to 497 ± 15 nm on sample after oxidation for 24 h at 300 °C.

A slightly different shape can be seen in chronopotentiometric curves in case of tin. The cathode potential sharply decreases, then increases, setting at a constant level, corresponding to the reduction of metal ions in the oxide, and then decreases to ca. -1.6 V in non-oxidizsed metals and to - 1.46 V in metals oxidised at 200 °C for 1 h and

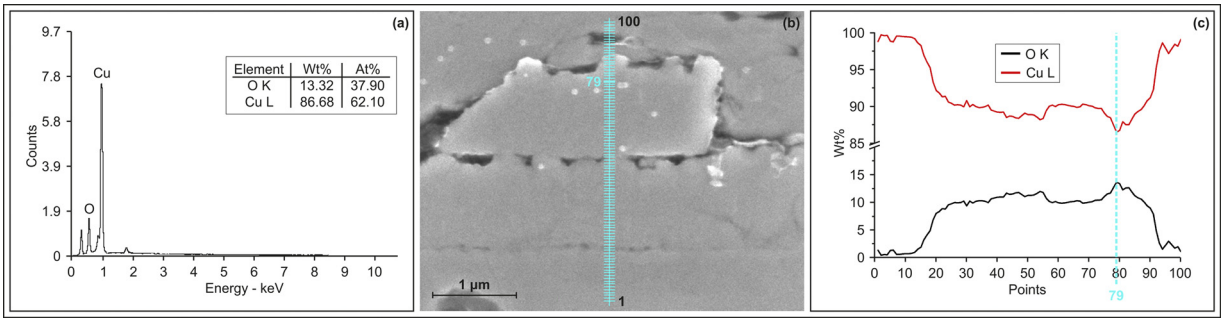

Fig. 10. Chemical composition of oxide layer on C11000 substrate: (a) Spectrograms containing spectra of characteristic x-ray radiation, and tables showing chemical composition (wt% and at%) of selected point, (b) SEM image of the analysed area, (c) EDX multipoint analysis of oxide layers on the surface.

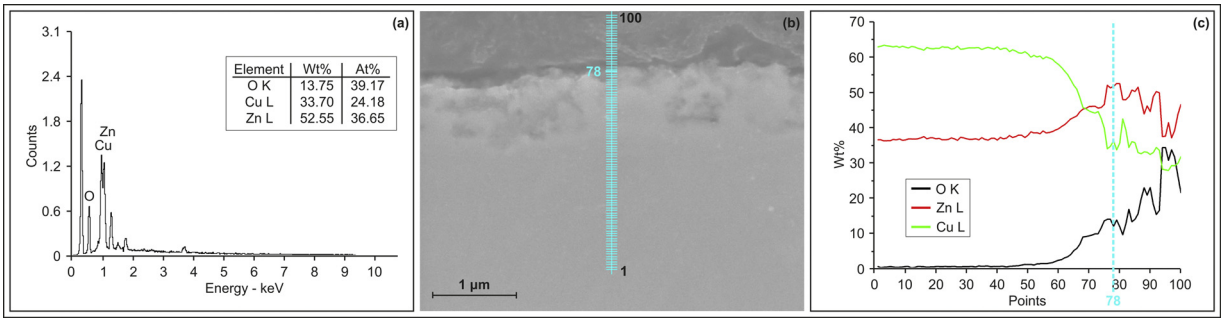

Fig. 11. Chemical composition of oxide layer on C27400 substrate: (a) Spectrograms containing spectra of characteristic x-ray radiation, and tables showing chemical composition (wt% and at%) of selected point, (b) SEM image of the analysed area, (c) EDX multipoint analysis of oxide layers on the surface.

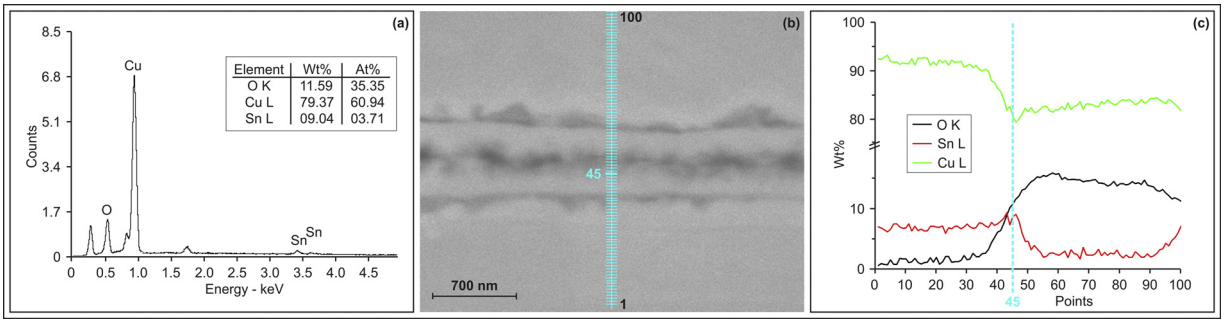

Fig. 12. Chemical composition of oxide layer on C51900 substrate: (a) Spectrograms containing spectra of characteristic x-ray radiation, and tables showing chemical composition (wt% and at%) of selected point, (b) SEM image of the analysed area, (c) EDX multipoint analysis of oxide layers on the surface.

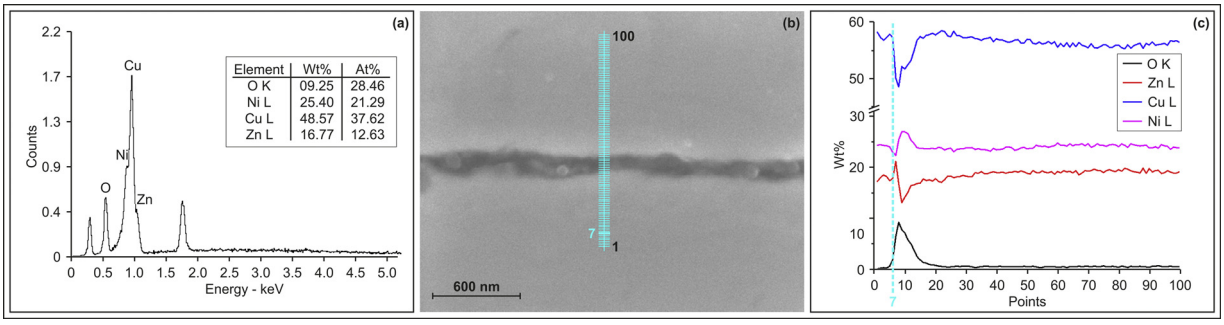

Fig. 13. Chemical composition of oxide layer on C75200 substrate: (a) Spectrograms containing spectra of characteristic x-ray radiation, and tables showing chemical composition (wt% and at%) of selected point, (b) SEM image of the analysed area, (c) EDX multipoint analysis of oxide layers on the surface.

24 h. The time interval that may correspond to oxide reduction oxide ranges from ca. 5 s for non-heat treated samples up to ca. 160 s for samples oxidised for 24 h. It was assumed that in these oxidation conditions only SnO is formed (SnO is the only oxide forming on tin oxidised at temperatures below 300 °C, above 300 °C, SnO degrades into Sn and SnO_2). Process of reduction of tin ions contained in SnO that occurs during electrolysis can be described by the following formula:

$$Sn^{2+} + 2e \rightarrow Sn \quad (16)$$

which was adopted as the basis for the calculation of the oxide layer

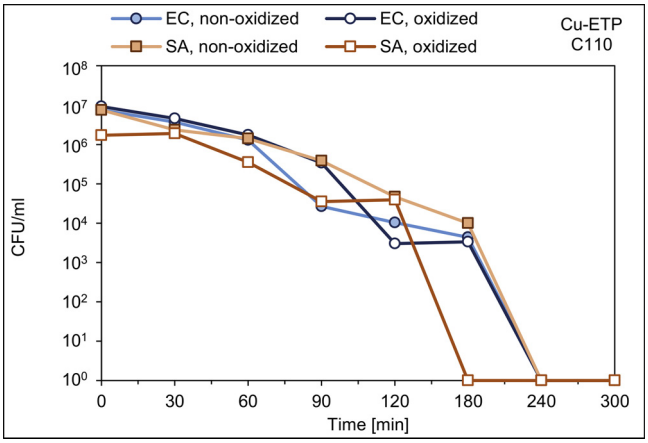

Fig. 14. Escherichia Coli (EC) and Staphylococcus Aureus (SA) suspension density (CFU/ml) reduction on oxidized (300 °C/1 h) and non-oxidised ETP copper (C11000).

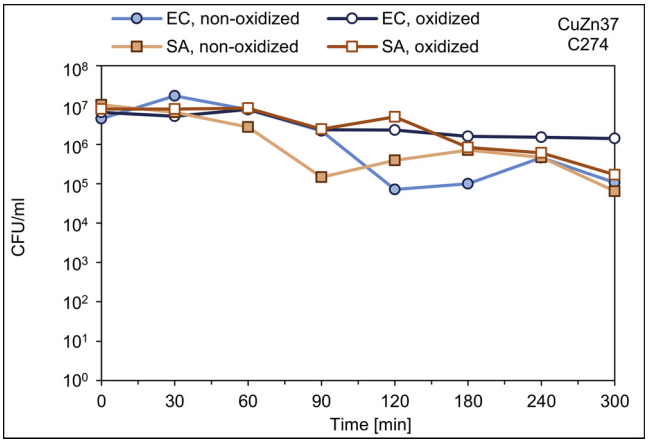

Fig. 15. Escherichia Coli (EC) and Staphylococcus Aureus (SA) suspension density (CFU/ml) reduction on oxidized (300 °C/24 h) and non-oxidised CuZn37 brass (C27400).

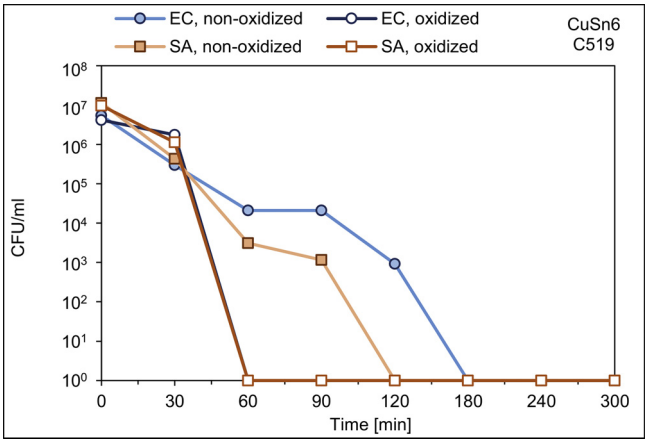

Fig. 16. Escherichia Coli (EC) and Staphylococcus Aureus (SA) suspension density (CFU/ml) reduction on oxidized (200 °C/1 h) and non-oxidised CuSn6 brass (C51900).

thickness by Eqs. (4) and (7), where d_{SnO} = 6.45 g/cm^3. The results obtained indicate that SnO thickness varies from 78 ± 6 nm (natural oxide layer) to 2639 ± 174 nm on tin oxidised for 24 h at 200 °C.

The potential-time curves obtained during the reduction of the oxide film on zinc depend on the oxidation conditions. For non-oxidised

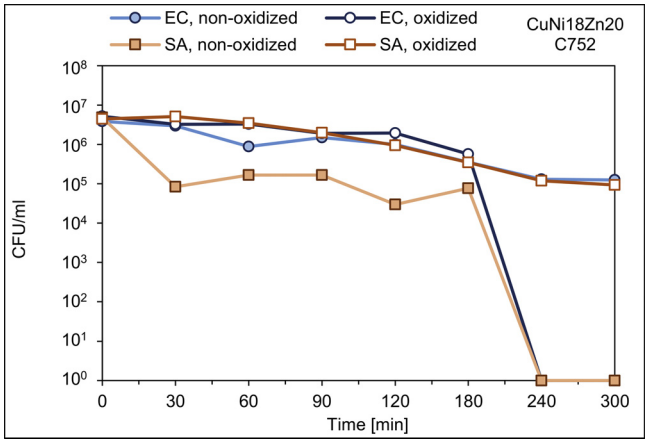

Fig. 17. Escherichia Coli (EC) and Staphylococcus Aureus (SA) suspension density (CFU/ml) reduction on oxidized (300 °C/24 h) and non-oxidised CuNi18Zn20 nickel-silver (C75200).

samples, after turning on the power for electrolysis, the cathode potential decreases to the plateau value at ca. -1.45 V, followed by a potential drop to the plateau within a range from -1.7 V to 1.8 V, associated with hydrogen ion reduction. Under these conditions, ZnO time reduction (ZnO formed at temperatures below 150–419 °C) is 10–15 s, which corresponds to the thickness of an oxide layer at ca. 100 nm. For oxidised metals, the curve shapes are not unambiguous. The likely timeframe that can correspond to oxide reduction is within ca. 145–210 s. Process of reduction of zinc ions contained in ZnO that occurs during electrolysis can be described by the following formula:

$$Zn^{2+} + 2e \rightarrow Zn \quad (17)$$

which was adopted as the basis for the calculation of the oxide layer thickness by Eqs. (4) and (7), where d_{ZnO} = 5.61 g/cm^3.

Fig. 7 presents potential-time curves for copper alloys with nickel and/or zinc and tin. Interpretation of obtained results without additional testing (phase analysis presented later in the paper) does not allow, at this stage, an unambiguous definition of the composition. Comparison of the curves obtained for alloys and pure metals indicates that the likely composition of oxide layers on copper alloys contains copper oxides. The results of the analysis for C27400, C51900 and C75200 alloys are is summarised in Table 4.

3.3. Multipoint quantitative chemical composition analysis (EDX multipoint)

The results of the EDX chemical composition analysis for selected areas/points on all test samples were grouped in the following order:

SEM images of sample cross-sections,

qualitative analysis - maps showing distribution of analysed elements,

"multipoint" quantitative analysis along a user-defined measurement lines coupled with graphs showing the concentration changes of analysed elements (wt.%),

EDS spectrograms and chemical composition tables (wt.% and at.%) with microphotographs for each of the analysed areas.

After the oxidation process (C11000: 300 °C / 1 h; C51900: 200 °C / 24 h; C27400, and C75200: 300 °C / 24 h) the revealed structure of oxide layers formed on metal substrates was observed using SEM. Figs. 8a-9d show surfaces of copper C11000 and C27400, C51900, C75200 alloys. The product Cu_2O layer for C11000 is ≈ 1.0 µm thick while for other alloys it is noticeably thinner: ≈ 650 nm for C27400, ≈ 300 nm for C51900, and ≈100 nm for C75200. These values comply with the results of the cathodic reduction tests.

Copper and copper alloys were also analysed for the distribution of

Table 5
The results of reduction of Staphylococcus Aureus (SA) and *Escherichia* Coli (EC) bacteria by copper and copper alloys.

Material	*Staphylococcus Aureus* (SA)		*Escherichia Coli* (EC)	
	Type of surface treatment of tested materials: thermal treatment			
	Surface non-oxidised	Surface oxidised	Non-oxidised surface	Oxidised surface
Copper Cu-ETP	Total reduction of suspension density after 240 min	Total reduction of suspension density after 180 min	Total reduction of suspension density after 240 min	Total reduction of suspension density after 240 min
Brass CuZn37	Reduction of output suspension density by ca. 2 log after 300 min	Reduction of output suspension density by ca. 2 log after 300 min	Reduction of output suspension density by ca. 2 log after 300 min	Reduction of output suspension density by ca. 1 log after 300 min
Tin bronze CuSn6	Total reduction of suspension density after 120 min	Total reduction of suspension density after 60 min	Total reduction of suspension density after 180 min	Total reduction of suspension density after 60 min
High nickel content brass (new silver) CuNi18Zn20	Total reduction of suspension density after 240 min	Reduction of output suspension density by ca. 2 log after 300 min	Reduction of output suspension density by ca. 2 log after 300 min	Total reduction of suspension density after 240 min

specified elements at the cross-section surfaces: O (radiation characteristic of K-series) and Cu, Zn, Sn, Ni (radiation characteristic of K and L series). Relevant maps with detected elements are presented in Fig. 9.

Previously observed samples of oxidized layers (copper and its alloys) were thoroughly analysed for the presence of chosen elements using the multipoint method along a defined measurement line (through the cross-sections). Figs. 10–13b presents mentioned cross-sections of C11000, C27400, C51900, and C75200 respectively. Materials in the form of flat sheets with oxidised surfaces were coupled together for the SEM observations and the measurement line for 100 points was drawn. Figs. 10–13c presents charts showing changes in concentrations of analysed elements (wt%) along the line. Content of Cu, O, and other alloy additives varies on cross-sections from the core (metal substrate), through oxide layers in the middle to upper substrate. The highest copper content in the material core decreases in the direction of the oxide layers at the expense of build-up of oxygen and other additives. For selected measurement points along a defined line spectrograms of characteristic x-ray radiation are shown in Figs. 10–13a.

3.4. Results of microbiological tests on antimicrobial efficiency

After the oxidation, copper C11000 and its alloys: C51900, C27400, and C75200 were tested for antimicrobial efficiency in contact with bacteria of Staphylococcus Aureus (SA) and *Escherichia* Coli (EC). Figs. 14–17 presents a reduction in bacteria count on non-oxidised and oxidised samples (C11000: 300 °C/1 h; C51900: 200 °C / 24 h; C27400, and C75200: 300 °C / 24 h). A summary of results is shown in Table 5.

For oxidized ETP copper (see Fig. 14) complete reduction of the SA bacteria count occurred after 180 min, while in case of non-oxidised ETP copper – after 240 min. The reduction time for EC suspension was the same for this material regardless of its surface condition – 240 min. For non-oxidised and oxidized brass CuZn37, (see Fig. 15), 2 log reduction was observed for SA after 300 min, while for EC – the total bacteria reduction was by ca. 1 log. Difference in antimicrobial performance between non-oxidized and oxidized brass was not found. In case of CuSn6 tin bronze, the total bacteria count reduction for a oxidised material (see Fig. 16) both for SA and EC, occurred after 60 min. For non-oxidised CuSn6 alloy, total reduction time was much longer for both bacteria types and it was 120 min for SA, and 180 min for EC. For nickel-silver CuNi18Zn20 (see Fig. 17), a bacteria total reduction occurred after 240 min for SA on non-oxidised surface, and for EC after an oxidation process.

4. Conclusions

As it was shown in the literature analysis the corrosion products on copper based touch surfaces are mostly copper oxides, which can be explained by the fact that other chemical compounds (chlorides, etc.) are not resistant to repeated wear by human palms. This research is based on the assumption that by means of atmospheric oxidation it is possible to produce oxide layers, which are similar to those reported after real life human palm oxidation. On the basis of conducted experiments on atmospheric oxidation and detailed characterization of the obtained surface layer parameters it was found these layers at properly selected heat treatment parameters can simulate oxide layers produced by contact with human palm sweat. On basis of microbiological tests of chosen oxidized and non-oxidized test samples it was found that oxidation has very little to none effect on antimicrobial efficiency of test materials. Only in case of tin bronze visible improvement after oxidation can be seen in comparison to non-oxidized surfaces.

Author contributions

Monika Walkowicz planned the experiments, performed corrosion experiments, performed annealing experiments, analysed and interpreted the data, and was a major contributor to the writing of the manuscript.

Piotr Osuch planned the experiments, performed annealing experiments, performed SEM-microscopic observations and EDX analysis, analysed and interpreted the data, prepared artwork for publication.

Beata Smyrak performed corrosion experiments, analysed and interpreted the data, drafted the manuscript

Tadeusz Knych analysed and interpreted the data, drafted the manuscript.

Ewa Rudnik performed chronopotentiometric measurements, analysed and interpreted the data.

Łukasz Cieniek performed SEM-microscopic observations and EDX analysis, analysed and interpreted the data

Anna Różańska performed laboratory microbiological tests, analysed and interpreted the data, drafted the manuscript.

Agnieszka Chmielarczyk performed laboratory microbiological tests, analysed and interpreted the data, drafted the manuscript.

Dorota Romaniszyn performed laboratory microbiological tests, analysed and interpreted the data, drafted the manuscript.

Małgorzata Bulanda analysed and interpreted the data, drafted the manuscript.

Conflicts of interest

The authors declare no conflict of interest.

Acknowledgements

This work was supported by The National Centre for Research and Development, Poland [grant number PBS3/A9/32/2015]. The authors also thank Prof. Marek Blicharski for his contribution to microscopy experiments.

References

[1] International Copper Association, Antimicrobial Copper Logo and Cu + Mark, the Conditions of Use, (2015) (Accessed 19 June 2017), http://www.antimicrobialcopper.org/sites/default/files/orig/media/83761/amc-conditions-of-use.pdf.
[2] A. Mikolay, S. Huggett, L. Tikana, G. Grass, J. Braun, D.H. Nies, Survival of bacteria on metallic surfaces in a hospital trial, Appl. Microbiol. Biotechnol. 87 (2010) 1875–1879.
[3] J.O. Noyce, H. Michels, C.W. Keevil, Potential use of copper surfaces to reduce survival of epidemic meticillin-resistant *Staphylococcus aureus* in the healthcare environment, J. Hosp. Infect. 63 (2006) 289–297.
[4] L. Weaver, H.T. Michels, C.W. Keevil, Survival of clostridium difficile on copper and steel: futuristic options for hospital hygiene, J. Hosp. Infect. 68 (2008) 145–151.
[5] S.L. Warnes, S.M. Green, H.T. Michels, C.W. Keevil, Biocidal efficacy of copper alloys against pathogenic enterococci involves degradation of genomic and plasmid DNAs, Appl. Environ. Microbiol. 76 (2010) 5390–5401.
[6] Japanese, Antimicrobial Products-Test for Antimicrobial Activity and Efficacy, JIS Z 2801:2000, in: Japanese Industrial Standard, (2000).
[7] H.T. Michels, D.G. Anderson, J.O. Noyce, S.A. Wilks, C.W. Keevil, The antimicrobial properties of copper alloys and their potential applications, in: J. Hugens, K. Sadayappan, J. Sponner, L.D. Smith, C. Twigge Molecey, J. Kale, A. Fuwa (Eds.), Plenary/Copper and Alloy Casting and Fabrication/Copper-Economics and Markets, Piret, Toronto, Canada, 2007.
[8] B. Keevil, S. Warnes, New insights into the antimicrobial mechanisms of copper touch surfaces, BMC Proc. 5 (Suppl 6) (2011) P39.
[9] X. Wei, Y. Yang, S.L. Wang, w. Tay, Gao, Polymer antimicrobial coatings with embedded fine Cu and Cu salt particles, Appl. Microbiol. Biotechnol. 98 (2014) 6265–6274.
[10] G. Grass, Ch. Rensing, M. Solioz, Metallic copper as an antimicrobial surface, Appl. Environ. Microbiol. 77 (2011) 1541–1547.
[11] S. Mathews, M. Hans, F. Mucklich, M. Solioz, Contact killing of bacteria on copper is suppressed if bacterial-metal contact is prevented and is induced on the iron to copper ions, Appl. Environ. Microbiol. 98 (2013) 1–7.
[12] D.J. Horton, H. Ha, L.L. Foster, H.J. Bindig, J.R. Scully, Tarnishing and Cu ion release in selected copper-base alloys: implications towards antimicrobial functionality, Electrochim. Acta 169 (2015) 351–366.
[13] Y. Zhu, K. Mimura, M. Isshiki, Oxidation mechanism of copper at 623-1073, K. Mater. Trans. 43 (2002) 2173–2176.
[14] J.H. Payer, Corrosion process in the development of thin tarnish films, Thirty-Sixth IEEE Conference on Electrical Contacts and the Fifteenth International Conference on Electrical Contacts, (1990), pp. 203–211.
[15] N. Fredj, J.S. Kolar, D.M. Prichard, Etc. Burleigh, Study of relative color stability and corrosion resistance of commercial copper alloys exposed to hand contact and synthetic hand sweat, Corros. Sci. 76 (2013) 415–423.
[16] C.J. Harvey, R.F. LeBouf, A.B. Stefaniak, Formulation and stability of a novel artificial human sweat under conditions of storage and use, Toxicol. In Vitro 24 (2010) 1790–1796.
[17] British, Reference Test Method for Release of Nickel from All Post Assemblies Which Are Inserted into Pierced Parts of the Human Body and Articles Intended to Come into Direct and Prolonged Contact With the Skin, BS EN 1811:2011 + A1:2015-09, in: British Standard (2011).
[18] ISO, Watch Cases and Accessories – Gold Alloy Coverings, in Part 2: Determination of Fineness, Thickness, Corrosion Resistance and Adhesion, ISO 3160-2:2000, in: International Standard (2000).
[19] I. Milošev, T. Kosec, Metal ion release and surface composition of the Cu-18Ni-20Zn nickel-silver during 30 days immersion in artificial sweat, Appl. Surf. Sci. 254 (2007) 644–652.
[20] S. Colin, E. Beche, R. Berjoan, H. Jolibois, A. Chambaudet, An XPS and AES study of the free corrosion of Cu-, Ni- and Zn-based alloys in synthetic sweat, Corros. Sci. 41 (1999) 1051–1065.
[21] R. Procaccini, W.H. Schreiner, M. Vázquez, S. Ceré, Surface study of films formed on copper and brass at open circuit potential, Appl. Surf. Sci. 268 (2013) 171–178.
[22] H. Elhadiri, K. Chegdani, M. Sobh, M. Cherkaoui, E.H. Rifi, Study of the behaviour of Moroccan coin ½ DH in a simulated sweat solution and 3% NaCl, J. Mater. Environ. Sci. 5 (5) (2014) 1557–1564.
[23] A.-Ch. Yeh, Ch-Ch. Huang, Ch-Ch. Hsiao, T.-W. Chu, Y.-Ch. Yang, Y.-W. Feng, K.-Y. Lin, Some aspects on the discoloration and antimicrobial property of a thermally passivated copper surface in a highly humid environment, Mater. Trans. 52 (2011) 265–267.
[24] H.T. Michels, S.A. Wilks, J.O. Noyce, C.W. Keevil, Copper alloys for human infectious disease control, Materials Science and Technology Conference, September 25–28, Pittsburgh, PA, Copper for the 21st Century Symposium, 2005.
[25] M. Souli, I. Galani, D. Plachouras, T. Panagea, A. Armaganidis, G. Petrikkos, H. Giamarellou, Antimicrobial activity of copper surfaces against carbapenemase-producing contemporarty Gram-negative clinical isolates, J. Antimicrob. Chemother. 68 (2013) 852–857.